ACS Catalysis

pubs.acs.org/acscatalysis Letter

CdS Quantum Dots for Metallaphotoredox-Enabled Cross-Electrophile Coupling of Aryl Halides with Alkyl Halides

Julianna M. Mouat, Jonas K. Widness, Daniel G. Enny, Mahilet T. Meidenbauer, Farwa Awan, Todd D. Krauss,* and Daniel J. Weix*

Cite This: ACS Catal. 2023, 13, 9018−9024 Read Online

ACCESS | Metrics & More | Article Recommendations | Supporting Information

ABSTRACT: Semiconductor quantum dots (QDs) offer many advantages as photocatalysts for synthetic photoredox catalysis, but no reports have explored the use of QDs with nickel catalysts for C−C bond formation. We show here that 5.7 nm CdS QDs are robust photocatalysts for photoredox-promoted cross-electrophile coupling (turnover number (TON) up to 40,000). These conditions can be utilized on a small scale (96-well plate) or adapted to flow. NMR studies show that triethanolamine (TEOA)-capped QDs are the active catalyst and that TEOA can displace native phosphonate and carboxylate ligands, demonstrating the importance of the QD surface chemistry.

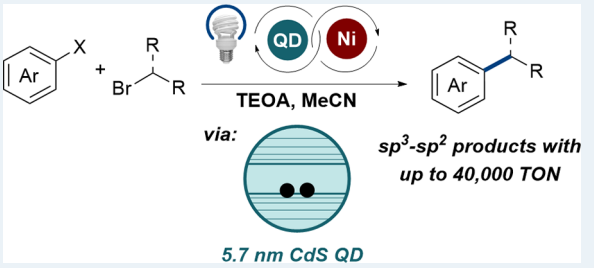

KEYWORDS: *quantum dot, nanoplatelet, nickel, cross-electrophile coupling, C−C bond formation, photochemistry*

Downloaded via UNIV ILLINOIS URBANA-CHAMPAIGN on July 21, 2023 at 00:23:45 (UTC).
See https://pubs.acs.org/sharingguidelines for options on how to legitimately share published articles.

Photoredox chemistry employing transition metal cocatalysts is a powerful strategy for C−C bond formation[1−3] but is generally limited by a small number of photoredox catalysts. For example, photoredox-promoted cross-electrophile coupling (PPXEC) procedures commonly require iridium-based dyes, stoichiometric use of expensive and high-molecular-weight silane reductants, or both (Scheme 1A).[4−11] Despite this, PPXEC is widely utilized on a small scale and would be an attractive approach to large-scale XEC if costs could be decreased. Both Vannucci's and Lei's PPXEC approaches avoided the need for silane reagents, which can be expensive and often introduce purification challenges, but required Ir dyes.[12,13] Precious-metal dyes are among the most developed metallaphotoredox catalysts, yet there are concerns surrounding the security of the platinum-group metal supply[14] and expense of these dyes at large scale. Recent reports have introduced organophotocatalysts, sometimes alongside non-silane reductants,[15−18] but these catalysts are also expensive for large-scale use and often require higher catalyst loadings. There is a need for scalable PPXEC catalysts that do not suffer from these hurdles.

Our group and others have evaluated semiconductor quantum dots (QDs) as replacements for precious-metal dyes in a variety of photoredox[19−23] and redox-neutral metallaphotoredox reactions,[20,24−26] but their viability for reductive metallaphotoredox catalysis remains unexplored (Scheme 1B). QDs could be an ideal replacement for precious metals and organic dyes due to their tunable visible absorption,[27] large molar absorptivity coefficients,[28] well-defined syntheses from inexpensive precursors,[29,30] solution stability in organic solvents, and high photostability,[31−33] among other advantages.[34−38] However, we envisioned several challenges in realizing a QD-catalyzed PPXEC reaction. The low concentrations of QDs typically employed,[39,40] combined with shorter excited-state lifetimes,[41−43] could give sluggish bimolecular quenching with a metal cocatalyst. Second, QDs can bind or react with metal ions[44−46] and common organic functional groups,[47−49] and undesired side reactivity between the QDs, metal cocatalysts, and reactants could inhibit catalysis. Finally, given the wide array of available QDs and nanomaterials,[30] the choice of appropriate nanomaterial composition and morphology was not obvious. We report here a systematic investigation of the use of QDs in a model PPXEC reaction that illustrates that CdS QDs are as effective as small-molecule dyes (Scheme 1C). Binding studies reveal that the terminal reductant (triethanolamine), a reported QD ligand,[50−53] replaces the native QD ligands in situ, remodeling the QD surface for optimal reactivity.

To identify the optimal nanomaterial photocatalysts for PPXEC, we examined several nanomaterials (reported in mol % nanomaterial) of differing morphologies, sizes, and electronic/chemical characteristics (see Supporting Information (SI) section 2 for characterization details).[20,54−61] The 5.7 nm CdS QDs (size determined by TEM imaging; see SI section 2 for sizing details) were the most effective photo-

Received: May 2, 2023
Revised: June 16, 2023
Published: June 22, 2023

ACS Publications © 2023 American Chemical Society

Scheme 1. Nickel Photoredox Catalysis and Quantum Dots

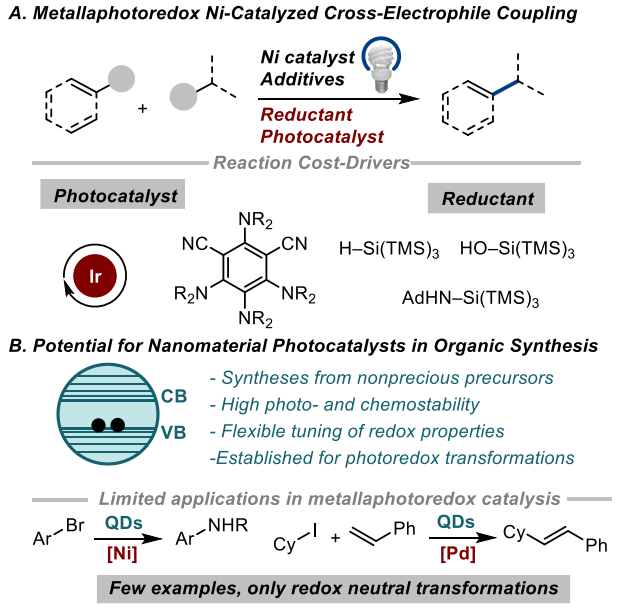

Table 1. Survey of Nanomaterial Photoredox Catalysts[a]

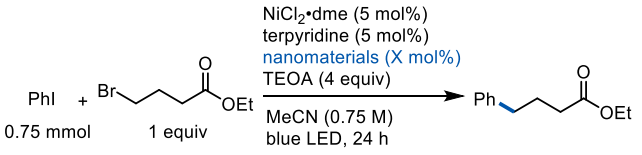

entry	nanomaterial photocatalyst	yield (%)[b]
1	5.7 nm CdS QDs (±0.72 nm) (2×10^{-3} mol %)	79 (80)[c]
2	5.3 nm CdS QDs (2×10^{-3} mol %)	67
3	4.9 nm CdS QDs (2×10^{-3} mol %)	64
4	3.9 nm CdS QDs, (2×10^{-3} mol %)	29
5	5.7 nm CdS QDs, 390 nm hν (2×10^{-3} mol %)	66
6	3.9 nm CdS QDs, 390 nm hν (2×10^{-3} mol %)	21
7	3.0 nm CdSe QDs (2×10^{-3} mol %)	4
8	2.2 nm CdSe QDs (2×10^{-3} mol %)	5
9	$CsPbBr_3$ bulk perovskite (10 mol %)	0
10	$CsPbBr_3$ perovskite QDs (1×10^{-3} mol %)	1
11	4.5 ML CdSe nanoplatelets (2×10^{-5} mol %)	10[d]
12	4.5 ML CdS nanoplatelets, 427 nm $h\nu$ (6×10^{-5} mol %)	35[d]
13	4.5 ML CdS nanoplatelets, 390 nm $h\nu$ (6×10^{-5} mol %)	34[d]
14	4.5 ML CdS nanoplatelets, 390 nm $h\nu$ (1.4×10^{-4} mol %)	53[d]

[a]Reactions were conducted at 0.75 mmol scale using 1 equiv of each coupling partner. The emission of the blue LEDs was centered around 447 nm. Catalyst loading is in mol % nanomaterial (e.g., QD, platelet). [b]Corrected GC yields. [c]Yield determined by ^{1}H NMR analysis. [d]48 h reaction time.

catalyst for this transformation (turnover number (TON) of ~40,000), while smaller CdS QDs gave lower yields of product and more dehalogenated arene (Table 1, entries 1−4). Employing higher-energy 390 nm irradiation to better excite

Table 2. Reaction Optimization Studies[a]

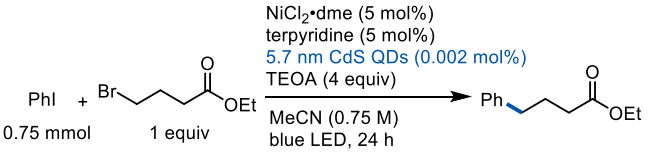

entry	variation	yield (%)[b]
1	none	79 (80)[c]
2	1 mol % [Ni] + ligand	60
3	2.5 equiv of TEOA	63
4	Hantzch ester instead of TEOA	ND
4	Et_3N instead of TEOA	19
5	DIPEA instead of TEOA	17
6	*N*-ethyldiethanolamine instead of TEOA	63
7	2-diethylaminoethanol instead of TEOA	16
8	2×10^{-4} mol % QDs	36
9	Bulk CdS (10 mol %) instead of QDs	13
10	omission of any one of Ni, ligand, reductant, light, or QDs	0

[a]Reactions conducted at 0.75 mmol scale using 1 equiv of each coupling partner. The emission of the blue LEDs was centered around 447 nm. [b]Corrected GC yields. [c]Yield determined by ^{1}H NMR analysis.

3.9 nm CdS QDs was also detrimental (Table 1, entries 5 and 6). Because dehalogenation has been associated with over-reduction of arylnickel(II) intermediates,[62] the increased amount of dehalogenation observed with smaller-diameter QDs suggests that larger band gap energies play a negative role. On the other hand, among different sized CdS QDs, the increased yield does not appear to be due to absorbance of more photons (see Figure S2). Overall, a number of size-dependent factors may account for the superior performance of the larger 5.7 nm CdS QDs compared to the other nanomaterials, including the extinction coefficients, band edge positions, and ligand coverage.

CdSe QDs, which exhibit smaller band gaps and lower valence band potentials than CdS,[27,63] did not provide the product in any appreciable yield (Table 1, entries 7 and 8), possibly due to insufficient driving force required for efficient oxidation of amine reductants. Both bulk and nanocrystalline $CsPbBr_3$ perovskites, possessing similar band gaps to 5.7 nm CdS, were completely ineffective (Table 1, entries 9 and 10), likely due to their rapid dissolution in polar environments unless functionalized with stabilizing ligands,[60] highlighting a fundamental challenge in the use of perovskite photocatalysts for organic chemistry. Preliminary attempts to use ~4.5 monolayer (ML) CdSe and CdS nanoplatelets, unexplored materials for metallaphotoredox catalysis, afforded promising yields (Table 1, entries 11−14) with very high total TONs (in some cases >500,000; see SI section 5 for details). While more concentrated nanoplatelet (NPL) solutions were problematic, comparison of NPLs with QDs at the same (lower) concentration demonstrated that NPLs can be more productive per particle (see Table S5). Due to the greater synthetic complexity of NPLs[64] and their lower initial performance, we opted to continue using 5.7 nm CdS QDs in this study. However, the high molar productivity of the NPLs suggests their significant potential as photoredox catalysts in future applications.

The optimized conditions employ $NiCl_2$(dme) with terpyridine as a ligand for Ni, utilizing triethanolamine

https://doi.org/10.1021/acscatal.3c01984
ACS Catal. 2023, 13, 9018−9024

Scheme 2. QD-Promoted Cross-Electrophile Coupling Reaction Scope and Scalability[h]

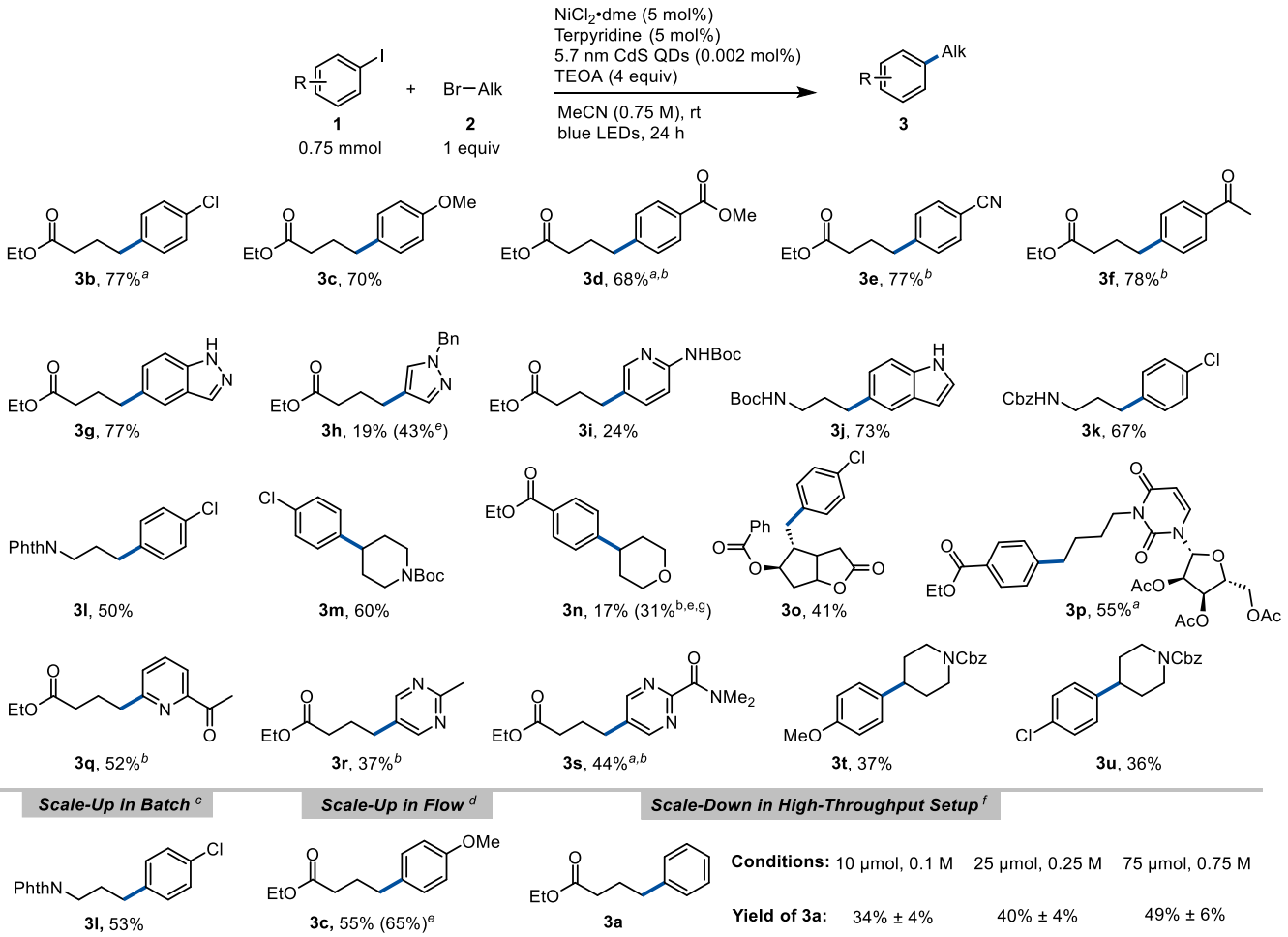

[h]Isolated yields after purification are reported, unless otherwise noted. See the SI for details. The emission of the blue LEDs was centered around 447 nm. [a]Product could not be fully isolated from impurities; the yield was determined via ^{1}H NMR spectroscopy. [b]Aryl bromide (1.5 equiv) was used instead of aryl iodide. [c]Conducted on a 5.0 mmol scale in batch. [d]Conducted on a 7.5 mmol scale using a flow setup. [e]^{1}H NMR yield before purification. [f]Conducted in 100 μL of MeCN in a well-plate setup. Corrected GC yields are reported. [g]Using 1 equiv of NaI.

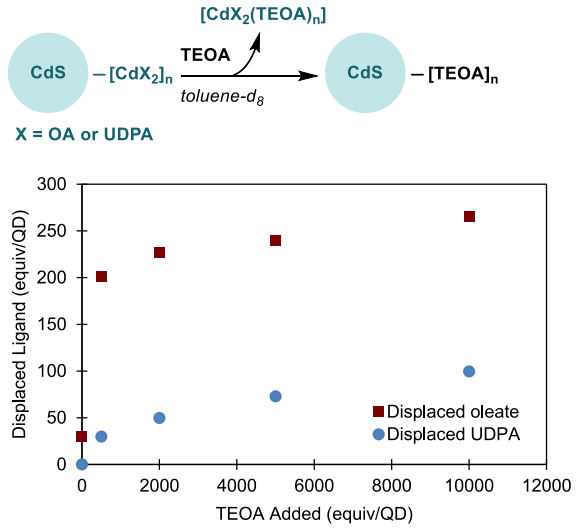

Figure 1. Displacement of native oleate (OA) ligands and undec-10-en-1-ylphosphonic acid (UDPA) from the surface of CdS QDs after treatment with triethanolamine (TEOA) in toluene-d_8. See SI section 4 for experimental details and NMR spectra.

(TEOA) as a homogeneous terminal reductant, with 5.7 nm CdS QDs (2.0×10^{-3} mol %) and blue LEDs. Reducing the loading of Ni/ligand or reductant produced diminished yields (Table 2, entries 1–3). Use of alternative tertiary amine reductants instead of TEOA gave greatly diminished yields despite exhibiting similar oxidation potentials[65−68] (Table 2, entries 4–7). Furthermore, the steady-state photoluminescence of the QDs was quenched to a greater extent by TEOA than DIPEA or Et_3N (SI section 5.2), consistent with its superior performance. Lowering the QD loading was detrimental, while bulk CdS powder was not an effective photocatalyst (Table 2, entries 8 and 9). Control experiments verified that all components were necessary for product formation (Table 2, entry 10).

We then briefly investigated the compatibility of the CdS QD/TEOA system with synthetically relevant substrates (Scheme 2). Electron-rich and -neutral aryl iodides were cross-coupled in good yields (**3a**–**3c**), while heteroaryl iodides including pyridine, indole, pyrazole, and indazole (**3g**–**3j**) could also be coupled. When electron-poor aryl iodides were used, significant amounts of hydrodehalogenated product were observed, consistent with the ability of CdX QDs (X = S, Se) to directly reduce electron-poor aryl iodides.[69] Electron-poor

https://doi.org/10.1021/acscatal.3c01984
ACS Catal. 2023, 13, 9018−9024

aryl bromides could also be coupled, albeit requiring 1.5 equiv of ArBr to achieve good yields (**3d**−**3f**). Following this trend, electron-poor heteroaryl moieties, including pyridine (**3q**) and pyrimidine (**3r**, **3s**), could be coupled in moderate yield. Additionally, both primary (**3a**−**3l**, **3o**, and **3p**) and secondary alkyl bromides (**3m**, **3n**, **3t**, and **3u**) could be coupled using this method. Synthetically valuable moieties, including halides, nitriles, ketones, esters, and protected amines, were generally well-tolerated. Corey lactone-derived **3o** and uridine-derived **3p** were afforded in good yields without the epimerization of chiral centers.

In the optimized reaction (Table 1, entry 1), the remainder of the mass balance was primarily protodehalogenation (PhH) with small amounts of remaining starting material and alkyl dimer. For the lower-yielding reactions in Scheme 2, protodehalogenation and alkyl dimerization were the main side products. For less reactive aryl halides, substantial amounts of the aryl halide remained.

The advantages of inexpensive production and robust solution stability render QDs an ideal photocatalyst platform for large-scale applications.[70] We found that **3l** could be scaled up to 5 mmol scale on the benchtop in batch mode, and **3c** could be scaled to 7.5 mmol in a flow reactor (Scheme 2). The latter reaction used only 0.001 mol % QDs (corresponding to a material cost of $0.26; see SI section 3.4 for details).

Furthermore, the reaction conditions could be readily applied to a smaller-scale, high-throughput format, utilizing a commercial 96-well plate equipped with a blue LED array on a shaker plate (see SI section 3.2 for details regarding setup and heat map data).

Modulation of the QD ligand environment by precursory exchange or in situ interactions with reaction components is known to strongly impact catalysis by changing the permeability of the ligand sphere.[71−74] To determine whether TEOA enables optimal QD performance through surface modification, we monitored the displacement of native oleate ligands from the QD surface upon treatment with TEOA via ^{1}H NMR spectroscopy (Figure 1). Alcohols have been proposed to undergo X-type ligand exchange with carboxylate QD ligands[75] but are not commonly employed as capping ligands for QDs.[76−78] Triethanolamine has been explored as a water-solubilizing ligand for QDs in sensing applications,[50,51] but ligand exchange dynamics and photocatalysis with TEOA-capped QDs have not been explored. Our ^{1}H NMR study showed oleate displacement from the QD surface by TEOA upon addition of TEOA equivalencies well below that of the catalytic reaction (Figures S4 and S7). Meanwhile, Et_3N and DIPEA displaced only a small fraction of the oleates on the QD surface (Figure S8). TEOA also displaced undec-10-en-1-ylphosphonic acid (UDPA) ligands from CdS (Figure S5). UDPA is known to bind more strongly than carboxylates to Cd sites on QD surfaces.[79] This similar efficacy of displacement together with TEOA's ability to form stable Cd(II) chelates[80] suggests that TEOA may remove ligands by chelation and stripping of surface-bound CdX_2 (X = UDPA or oleate) complexes rather than undergoing X-type ligand exchange.[81,82] Accompanying oleate displacement, a large negative nuclear Overhauser effect (NOE) correlation was observed between the methylene resonances of TEOA in the presence of QDs, indicating their dynamic association with the exposed QD surface following the displacement of surface-bound Cd(oleate)$_2$ (Figure S7).[83] While the binding mode of TEOA to the QD surface in this particular system remains unknown (i.e., L- vs X-type, binding through the amine vs hydroxyl moieties), our experiments are consistent with in situ formation of TEOA-capped QDs as the active catalyst under the optimal conditions (Figure 1). Structurally similar tertiary amines bearing zero or one hydroxyl group were less effective reductants, but two hydroxyl groups provided similar results (Table 2, entries 4−7), suggesting that some level of chelation is critical to function as a surface-remodeling reductant.[84]

In conclusion, we have demonstrated how CdS QDs with TEOA constitute a cost-effective photoreduction system for Ni-mediated cross-electrophile coupling that demonstrates a broad scope and good scalability. NMR studies illustrate the role of TEOA as a surface-binding reductant and how surface remodeling could be used to improve the reductive chemistry with QDs. Continuing studies on the use of nanomaterials for organic synthesis are ongoing and will be reported in due course.

■ ASSOCIATED CONTENT

Supporting Information

The Supporting Information is available free of charge at https://pubs.acs.org/doi/10.1021/acscatal.3c01984.

Additional optimization and characterization data, experimental procedures, and characterization data for all isolated compounds (PDF)

■ AUTHOR INFORMATION

Corresponding Authors

Daniel J. Weix − *Department of Chemistry, University of Wisconsin-Madison, Madison, Wisconsin 53706, United States;* orcid.org/0000-0002-9552-3378; Email: dweix@wisc.edu

Todd D. Krauss − *Department of Chemistry and Institute of Optics, University of Rochester, Rochester, New York 14627, United States;* orcid.org/0000-0002-4860-874X; Email: todd.krauss@rochester.edu

Authors

Julianna M. Mouat − *Department of Chemistry, University of Wisconsin-Madison, Madison, Wisconsin 53706, United States;* orcid.org/0000-0002-3976-3676

Jonas K. Widness − *Department of Chemistry, University of Wisconsin-Madison, Madison, Wisconsin 53706, United States;* orcid.org/0000-0002-7507-8254

Daniel G. Enny − *Department of Chemistry, University of Wisconsin-Madison, Madison, Wisconsin 53706, United States;* orcid.org/0000-0002-8644-4694

Mahilet T. Meidenbauer − *Materials Science Program, University of Rochester, Rochester, New York 14627, United States*

Farwa Awan − *Department of Chemistry, University of Rochester, Rochester, New York 14627, United States*

Complete contact information is available at: https://pubs.acs.org/10.1021/acscatal.3c01984

Notes

The authors declare no competing financial interest.

■ ACKNOWLEDGMENTS

This work was supported by the NIH (R21GM141622 to D.J.W. and T.D.K.), the NSF (CHE-1904847 to T.D.K.), the University of Wisconsin-Madison (D.J.W.), and the donors to

the Wayland E. Noland Chair (D.J.W.). The instrumentation in the PBCIC was supported as follows: Thermo Q Extractive Plus was supported by the NIH (1S10 OD020022); Shimadzu GCMS-QP2010S was supported by the Department of Chemistry; and Bruker Avance III 500 was supported by a generous gift from Paul J. and Margaret M. Bender. The authors thank the Yoon group (UW-Madison) for helpful discussions about photoluminescence quenching experiments and for access to their chemical inventory and supplies. They also thank Prof. Jillian Dempsey, Jennica Kelm, and Christian Dones-LaSalle (University of North Carolina-Chapel Hill) for guidance with NMR experiments.

REFERENCES

(1) Chan, A. Y.; Perry, I. B.; Bissonnette, N. B.; Buksh, B. F.; Edwards, G. A.; Frye, L. I.; Garry, O. L.; Lavagnino, M. N.; Li, B. X.; Liang, Y.; Mao, E.; Millet, A.; Oakley, J. V.; Reed, N. L.; Sakai, H. A.; Seath, C. P.; MacMillan, D. W. C. Metallaphotoredox: The Merger of Photoredox and Transition Metal Catalysis. *Chem. Rev.* **2022**, *122*, 1485−1542.

(2) Hopkinson, M. N.; Sahoo, B.; Li, J.-L.; Glorius, F. Dual Catalysis Sees the Light: Combining Photoredox with Organo-, Acid, and Transition-Metal Catalysis. *Chem. - Eur. J.* **2014**, *20*, 3874−3886.

(3) Prier, C. K.; Rankic, D. A.; MacMillan, D. W. C. Visible Light Photoredox Catalysis with Transition Metal Complexes: Applications in Organic Synthesis. *Chem. Rev.* **2013**, *113*, 5322−5363.

(4) Sakai, H. A.; Liu, W.; Le, C.; MacMillan, D. W. C. Cross-Electrophile Coupling of Unactivated Alkyl Chlorides. *J. Am. Chem. Soc.* **2020**, *142*, 11691−11697.

(5) Zhang, P.; Le, C.; MacMillan, D. W. C. Silyl Radical Activation of Alkyl Halides in Metallaphotoredox Catalysis: A Unique Pathway for Cross-Electrophile Coupling. *J. Am. Chem. Soc.* **2016**, *138*, 8084−8087.

(6) Smith, R. T.; Zhang, X.; Rincón, J. A.; Agejas, J.; Mateos, C.; Barberis, M.; García-Cerrada, S.; de Frutos, O.; MacMillan, D. W. C. Metallaphotoredox-Catalyzed Cross-Electrophile C_{sp^3}−C_{sp^3} Coupling of Aliphatic Bromides. *J. Am. Chem. Soc.* **2018**, *140*, 17433−17438.

(7) Delgado, P.; Glass, R. J.; Geraci, G.; Duvadie, R.; Majumdar, D.; Robinson, R. I.; Elmaarouf, I.; Mikus, M.; Tan, K. L. Use of Green Solvents in Metallaphotoredox Cross-Electrophile Coupling Reactions Utilizing a Lipophilic Modified Dual Ir/Ni Catalyst System. *J. Org. Chem.* **2021**, *86*, 17428−17436.

(8) Juliá, F.; Constantin, T.; Leonori, D. Applications of Halogen-Atom Transfer (XAT) for the Generation of Carbon Radicals in Synthetic Photochemistry and Photocatalysis. *Chem. Rev.* **2022**, *122*, 2292−2352.

(9) Dewanji, A.; Bülow, R. F.; Rueping, M. Photoredox/Nickel Dual-Catalyzed Reductive Cross Coupling of Aryl Halides Using an Organic Reducing Agent. *Org. Lett.* **2020**, *22*, 1611−1617.

(10) Kerackian, T.; Reina, A.; Bouyssi, D.; Monteiro, N.; Amgoune, A. Silyl Radical Mediated Cross-Electrophile Coupling of *N*-Acyl-Imides with Alkyl Bromides under Photoredox/Nickel Dual Catalysis. *Org. Lett.* **2020**, *22*, 2240−2245.

(11) Yu, W.; Chen, L.; Tao, J.; Wang, T.; Fu, J. Dual Nickel- and Photoredox-Catalyzed Reductive Cross-Coupling of Aryl Vinyl Halides and Unactivated Tertiary Alkyl Bromides. *Chem. Commun.* **2019**, *55*, 5918−5921.

(12) Paul, A.; Smith, M. D.; Vannucci, A. K. Photoredox-Assisted Reductive Cross-Coupling: Mechanistic Insight into Catalytic Aryl−Alkyl Cross-Couplings. *J. Org. Chem.* **2017**, *82*, 1996−2003.

(13) Duan, Z.; Li, W.; Lei, A. Nickel-Catalyzed Reductive Cross-Coupling of Aryl Bromides with Alkyl Bromides: Et_3N as the Terminal Reductant. *Org. Lett.* **2016**, *18*, 4012−4015.

(14) Volz, D.; Wallesch, M.; Fléchon, C.; Danz, M.; Verma, A.; Navarro, J. M.; Zink, D. M.; Bräse, S.; Baumann, T. From Iridium and Platinum to Copper and Carbon: New Avenues for More Sustainability in Organic Light-Emitting Diodes. *Green Chem.* **2015**, *17*, 1988−2011.

(15) Luridiana, A.; Mazzarella, D.; Capaldo, L.; Rincón, J. A.; García-Losada, P.; Mateos, C.; Frederick, M. O.; Nuño, M.; Jan Buma, W.; Noël, T. The Merger of Benzophenone HAT Photocatalysis and Silyl Radical-Induced XAT Enables Both Nickel-Catalyzed Cross-Electrophile Coupling and 1,2-Dicarbofunctionalization of Olefins. *ACS Catal.* **2022**, *12*, 11216−11225.

(16) Lau, S. H.; Borden, M. A.; Steiman, T. J.; Wang, L. S.; Parasram, M.; Doyle, A. G. Ni/Photoredox-Catalyzed Enantioselective Cross-Electrophile Coupling of Styrene Oxides with Aryl Iodides. *J. Am. Chem. Soc.* **2021**, *143*, 15873−15881.

(17) Yedase, G. S.; Jha, A. K.; Yatham, V. R. Visible-Light Enabled $C(sp^3)$−$C(sp^2)$ Cross-Electrophile Coupling via Synergistic Halogen-Atom Transfer (XAT) and Nickel Catalysis. *J. Org. Chem.* **2022**, *87*, 5442−5450.

(18) Tian, X.; Kaur, J.; Yakubov, S.; Barham, J. P. α-Amino Radical Halogen Atom Transfer Agents for Metallaphotoredox-Catalyzed Cross-Electrophile Couplings of Distinct Organic Halides. *ChemSusChem* **2022**, *15*, No. e202200906.

(19) Widness, J. K.; Enny, D. G.; McFarlane-Connelly, K. S.; Miedenbauer, M. T.; Krauss, T. D.; Weix, D. J. CdS Quantum Dots as Potent Photoreductants for Organic Chemistry Enabled by Auger Processes. *J. Am. Chem. Soc.* **2022**, *144*, 12229−12246.

(20) Caputo, J. A.; Frenette, L. C.; Zhao, N.; Sowers, K. L.; Krauss, T. D.; Weix, D. J. General and Efficient C−C Bond Forming Photoredox Catalysis with Semiconductor Quantum Dots. *J. Am. Chem. Soc.* **2017**, *139*, 4250−4253.

(21) Huang, C.; Li, X.-B.; Tung, C.-H.; Wu, L.-Z. Photocatalysis with Quantum Dots and Visible Light for Effective Organic Synthesis. *Chem. - Eur. J.* **2018**, *24*, 11530−11534.

(22) Wu, H.-L.; Qi, M.-Y.; Tang, Z.-R.; Xu, Y.-J. Semiconductor Quantum Dots: A Versatile Platform for Photoredox Organic Transformation. *J. Mater. Chem. A* **2023**, *11*, 3262−3280.

(23) Yuan, Y.; Jin, N.; Saghy, P.; Dube, L.; Zhu, H.; Chen, O. Quantum Dot Photocatalysts for Organic Transformations. *J. Phys. Chem. Lett.* **2021**, *12*, 7180−7193.

(24) Zhang, Z.; Rogers, C. R.; Weiss, E. A. Energy Transfer from CdS QDs to a Photogenerated Pd Complex Enhances the Rate and Selectivity of a Pd-Photocatalyzed Heck Reaction. *J. Am. Chem. Soc.* **2020**, *142*, 495−501.

(25) Zhao, Z.; Reischauer, S.; Pieber, B.; Delbianco, M. Carbon Dot/TiO2 Nanocomposites as Photocatalysts for Metallaphotocatalytic Carbon−Heteroatom Cross-Couplings. *Green Chem.* **2021**, *23*, 4524−4530.

(26) Zhao, Z.; Pieber, B.; Delbianco, M. Modulating the Surface and Photophysical Properties of Carbon Dots to Access Colloidal Photocatalysts for Cross-Couplings. *ACS Catal* **2022**, *12*, 13831−13837.

(27) Jasieniak, J.; Califano, M.; Watkins, S. E. Size-Dependent Valence and Conduction Band-Edge Energies of Semiconductor Nanocrystals. *ACS Nano* **2011**, *5*, 5888−5902.

(28) Sun, J.; Goldys, E. M. Linear Absorption and Molar Extinction Coefficients in Direct Semiconductor Quantum Dots. *J. Phys. Chem. C* **2008**, *112*, 9261−9266.

(29) Reiss, P.; Carrière, M.; Lincheneau, C.; Vaure, L.; Tamang, S. Synthesis of Semiconductor Nanocrystals, Focusing on Nontoxic and Earth-Abundant Materials. *Chem. Rev.* **2016**, *116*, 10731−10819.

(30) Alivisatos, A. P. Semiconductor Clusters, Nanocrystals, and Quantum Dots. *Science* **1996**, *271*, 933.

(31) Soloviev, M. *Nanoparticles in Biology and Medicine: Methods and Protocols*; Springer: New York, 2020.

(32) Resch-Genger, U.; Grabolle, M.; Cavaliere-Jaricot, S.; Nitschke, R.; Nann, T. Quantum Dots versus Organic Dyes as Fluorescent Labels. *Nat. Methods* **2008**, *5*, 763−775.

(33) Gould, T. J.; Bewersdorf, J.; Hess, S. T. A Quantitative Comparison of the Photophysical Properties of Selected Quantum Dots and Organic Fluorophores. *Z. Phys. Chem.* **2008**, *222*, 833−849.

(34) Photocatalytic systems based on heterogeneous semiconductors constitute another promising platform for overcoming limitations of small-molecule photocatalysts. See the following references:

https://doi.org/10.1021/acscatal.3c01984
ACS Catal. 2023, 13, 9018−9024

(35) Gisbertz, S.; Pieber, B. Heterogeneous Photocatalysis in Organic Synthesis. *ChemPhotoChem* **2020**, *4*, 456−475.
(36) Dam, B.; Das, B.; Patel, B. K. Graphitic Carbon Nitride Materials in Dual Metallo-Photocatalysis: A Promising Concept in Organic Synthesis. *Green Chem.* **2023**, *25*, 3374−3397.
(37) Savateev, A.; Antonietti, M. Heterogeneous Organocatalysis for Photoredox Chemistry. *ACS Catal.* **2018**, *8*, 9790−9808.
(38) Marchi, M.; Gentile, G.; Rosso, C.; Melchionna, M.; Fornasiero, P.; Filippini, G.; Prato, M. The Nickel Age in Synthetic Dual Photocatalysis: A Bright Trip Toward Materials Science. *ChemSusChem* **2022**, *15*, No. e202201094.
(39) Arcudi, F.; Đorđević, L.; Nagasing, B.; Stupp, S. I.; Weiss, E. A. Quantum Dot-Sensitized Photoreduction of CO_2 in Water with Turnover Number > 80,000. *J. Am. Chem. Soc.* **2021**, *143*, 18131−18138.
(40) Feng, Y.-X.; Wang, H.-J.; Wang, J.-W.; Zhang, W.; Zhang, M.; Lu, T.-B. Stand-Alone CdS Nanocrystals for Photocatalytic CO2 Reduction with High Efficiency and Selectivity. *ACS Appl. Mater. Interfaces* **2021**, *13*, 26573−26580.
(41) Mi, C.; Saniepay, M.; Beaulac, R. Overcoming the Complex Excited-State Dynamics of Colloidal Cadmium Selenide Nanocrystals Involved in Energy Transfer Processes. *Chem. Mater.* **2018**, *30*, 5714−5725.
(42) Pu, C.; Qin, H.; Gao, Y.; Zhou, J.; Wang, P.; Peng, X. Synthetic Control of Exciton Behavior in Colloidal Quantum Dots. *J. Am. Chem. Soc.* **2017**, *139*, 3302−3311.
(43) Gammon, D.; Snow, E. S.; Katzer, D. S. Excited State Spectroscopy of Excitons in Single Quantum Dots. *Appl. Phys. Lett.* **1995**, *67*, 2391−2393.
(44) Jong, T.; Parry, D. L. Adsorption of Pb(II), Cu(II), Cd(II), Zn(II), Ni(II), Fe(II), and As(V) on Bacterially Produced Metal Sulfides. *J. Colloid Interface Sci.* **2004**, *275*, 61−71.
(45) Hörner, G.; Johne, P.; Künneth, R.; Twardzik, G.; Roth, H.; Clark, T.; Kisch, H. Semiconductor Type A Photocatalysis: Role of Substrate Adsorption and the Nature of Photoreactive Surface Sites in Zinc Sulfide Catalyzed C−C Coupling Reactions. *Chem. - Eur. J.* **1999**, *5*, 208−217.
(46) Davis, A. P.; Hsieh, Y. H.; Huang, C. P. Photo-Oxidative Dissolution of CdS(s): The Effect of Cu(II) Ions. *Chemosphere* **1994**, *28*, 663−674.
(47) Hines, D. A.; Kamat, P. V. Quantum Dot Surface Chemistry: Ligand Effects and Electron Transfer Reactions. *J. Phys. Chem. C* **2013**, *117*, 14418−14426.
(48) Kessler, M. L.; Starr, H. E.; Knauf, R. R.; Rountree, K. J.; Dempsey, J. L. Exchange Equilibria of Carboxylate-Terminated Ligands at PbS Nanocrystal Surfaces. *Phys. Chem. Chem. Phys.* **2018**, *20*, 23649−23655.
(49) Chen, P. E.; Anderson, N. C.; Norman, Z. M.; Owen, J. S. Tight Binding of Carboxylate, Phosphonate, and Carbamate Anions to Stoichiometric CdSe Nanocrystals. *J. Am. Chem. Soc.* **2017**, *139*, 3227−3236.
(50) Yan, X. Q.; Shang, Z. B.; Zhang, Z.; Wang, Y.; Jin, W. J. Fluorescence Sensing of Nitric Oxide in Aqueous Solution by Triethanolamine-Modified CdSe Quantum Dots. *Luminescence* **2009**, *24*, 255−259.
(51) Shang, Z. B.; Wang, Y.; Jin, W. J. Triethanolamine-Capped CdSe Quantum Dots as Fluorescent Sensors for Reciprocal Recognition of Mercury(II) and Iodide in Aqueous Solution. *Talanta* **2009**, *78*, 364−369.
(52) Dlamini, N. N.; Rajasekhar Pullabhotla, V. S. R.; Revaprasadu, N. Synthesis of Triethanolamine (TEA) Capped CdSe Nanoparticles. *Mater. Lett.* **2011**, *65*, 1283−1286.
(53) Dlamini, N. N.; Pullabhotla, V. S. R. R.; Revaprasadu, N. A Simple Route to Triethanolamine (TEA) and Cysteine Capped ZnSe Nanoparticles. *J. Nanosci. Nanotechnol.* **2012**, *12*, 2645−2651.
(54) Liu, Y.-Y.; Liang, D.; Lu, L.-Q.; Xiao, W.-J. Practical Heterogeneous Photoredox/Nickel Dual Catalysis for C−N and C−O Coupling Reactions. *Chem. Commun.* **2019**, *55*, 4853−4856.
(55) Li, J.-Y.; Li, Y.-H.; Qi, M.-Y.; Lin, Q.; Tang, Z.-R.; Xu, Y.-J. Selective Organic Transformations over Cadmium Sulfide-Based Photocatalysts. *ACS Catal.* **2020**, *10*, 6262−6280.
(56) Li, X.-B.; Li, Z.-J.; Gao, Y.-J.; Meng, Q.-Y.; Yu, S.; Weiss, R. G.; Tung, C.-H.; Wu, L.-Z. Mechanistic Insights into the Interface-Directed Transformation of Thiols into Disulfides and Molecular Hydrogen by Visible-Light Irradiation of Quantum Dots. *Angew. Chem., Int. Ed.* **2014**, *53*, 2085−2089.
(57) Zhu, X.; Lin, Y.; San Martin, J.; Sun, Y.; Zhu, D.; Yan, Y. Lead Halide Perovskites for Photocatalytic Organic Synthesis. *Nat. Commun.* **2019**, *10*, 2843.
(58) Jones, L. O.; Mosquera, M. A.; Jiang, Y.; Weiss, E. A.; Schatz, G. C.; Ratner, M. A. Thermodynamics and Mechanism of a Photocatalyzed Stereoselective [2 + 2] Cycloaddition on a CdSe Quantum Dot. *J. Am. Chem. Soc.* **2020**, *142*, 15488−15495.
(59) Jiang, Y.; López-Arteaga, R.; Weiss, E. A. Quantum Dots Photocatalyze Intermolecular [2 + 2] Cycloadditions of Aromatic Alkenes Adsorbed to Their Surfaces via van Der Waals Interactions. *J. Am. Chem. Soc.* **2022**, *144*, 3782−3786.
(60) Hu, H.; Chen, M.; Yao, N.; Wu, L.; Zhong, Q.; Song, B.; Cao, M.; Zhang, Q. Highly Stable $CsPbBr_3$ Colloidal Nanocrystal Clusters as Photocatalysts in Polar Solvents. *ACS Appl. Mater. Interfaces* **2021**, *13*, 4017−4025.
(61) Chauviré, T.; Mouesca, J.-M.; Gasparutto, D.; Ravanat, J.-L.; Lebrun, C.; Gromova, M.; Jouneau, P.-H.; Chauvin, J.; Gambarelli, S.; Maurel, V. Redox Photocatalysis with Water-Soluble Core−Shell CdSe-ZnS Quantum Dots. *J. Phys. Chem. C* **2015**, *119*, 17857−17866.
(62) Truesdell, B. L.; Hamby, T. B.; Sevov, C. S. General $C(sp^2)$−$C(sp^3)$ Cross-Electrophile Coupling Reactions Enabled by Overcharge Protection of Homogeneous Electrocatalysts. *J. Am. Chem. Soc.* **2020**, *142*, 5884−5893.
(63) Dabbous, A.; Colson, E.; Chakravorty, D.; Mouesca, J.-M.; Lombard, C.; Caillat, S.; Ravanat, J.-L.; Dubois, F.; Dénès, F.; Renaud, P.; Maurel, V. Fine Tuning of Quantum Dots Photocatalysts for the Synthesis of Tropane Alkaloid Skeletons. *Chem. - Eur. J.* **2023**, *29*, No. e202300303.
(64) Diroll, B. T.; Guzelturk, B.; Po, H.; Dabard, C.; Fu, N.; Makke, L.; Lhuillier, E.; Ithurria, S. 2D II−VI Semiconductor Nanoplatelets: From Material Synthesis to Optoelectronic Integration. *Chem. Rev.* **2023**, *123*, 3543−3624.
(65) Small differences in the reported oxidation potentials of TEOA (+0.68 V vs SCE), DIPEA (+0.63 V vs SCE), and triethylamine (+0.80 V vs SCE) are inconsistent with their differences in catalytic performance.
(66) Kamada, K.; Jung, J.; Wakabayashi, T.; Sekizawa, K.; Sato, S.; Morikawa, T.; Fukuzumi, S.; Saito, S. Photocatalytic CO_2 Reduction Using a Robust Multifunctional Iridium Complex toward the Selective Formation of Formic Acid. *J. Am. Chem. Soc.* **2020**, *142*, 10261−10266.
(67) Chen, F.; Hu, S.; Li, S.; Tang, G.; Zhao, Y. Visible-Light-Induced Denitrogenative Phosphorylation of Benzotriazinones: A Metal- and Additive-Free Method for Accessing Ortho-Phosphorylated Benzamide Derivatives. *Green Chem.* **2021**, *23*, 296−301.
(68) Tian, H.; Shimakoshi, H.; Park, G.; Kim, S.; You, Y.; Hisaeda, Y. Photocatalytic Function of the B12 Complex with the Cyclometalated Iridium(Iii) Complex as a Photosensitizer under Visible Light Irradiation. *Dalton Trans.* **2018**, *47*, 675−683.
(69) Pal, A.; Ghosh, I.; Sapra, S.; Koenig, B. Quantum Dots in Visible-Light Photoredox Catalysis: Reductive Dehalogenations and C-H Arylation Reactions Using Aryl Bromides. *Chem. Mater.* **2017**, *29*, 5225−5231.
(70) Objective cost comparisons for photocatalyst use are challenging. Our optimal QDs are not yet commercially available, while the final costs of using molecular photocatalysts depend on catalyst sourcing, loading, and purification considerations. However, the bulk prices of respective precursor materials are illustrative: CdS QDs are produced using CdO ($14/mol, Alfa Aesar) and sulfur (<1¢/mol). Ir photocatalysts are usually produced from $IrCl_3$ ($57,660/mol, Pressure Chemical) and heteroaromatic organic

https://doi.org/10.1021/acscatal.3c01984
ACS Catal. 2023, 13, 9018−9024

ligands which impart variable synthetic costs. Isophthalonitrile photocatalysts are typically prepared from tetrafluoroisophthalonitrile ($1,376/mol, Ambeed) and various aromatic amines. Moreover, CdS QDs can be prepared in a single step and isolated without chromatography.

(71) Zhang, Z.; Edme, K.; Lian, S.; Weiss, E. A. Enhancing the Rate of Quantum-Dot-Photocatalyzed Carbon−Carbon Coupling by Tuning the Composition of the Dot's Ligand Shell. *J. Am. Chem. Soc.* **2017**, *139*, 4246−4249.

(72) Nepomnyashchii, A. B.; Harris, R. D.; Weiss, E. A. Composition and Permeability of Oleate Adlayers of CdS Quantum Dots upon Dilution to Photoluminescence-Relevant Concentrations. *Anal. Chem.* **2016**, *88*, 3310−3316.

(73) Weinberg, D. J.; He, C.; Weiss, E. A. Control of the Redox Activity of Quantum Dots through Introduction of Fluoroalkanethiolates into Their Ligand Shells. *J. Am. Chem. Soc.* **2016**, *138*, 2319−2326.

(74) Chang, C. M.; Orchard, K. L.; Martindale, B. C. M.; Reisner, E. Ligand Removal from CdS Quantum Dots for Enhanced Photocatalytic H_2 Generation in pH Neutral Water. *J. Mater. Chem. A* **2016**, *4*, 2856−2862.

(75) Hassinen, A.; Moreels, I.; De Nolf, K.; Smet, P. F.; Martins, J. C.; Hens, Z. Short-Chain Alcohols Strip X-Type Ligands and Quench the Luminescence of PbSe and CdSe Quantum Dots, Acetonitrile Does Not. *J. Am. Chem. Soc.* **2012**, *134*, 20705−20712.

(76) Owen, J. S.; Park, J.; Trudeau, P.-E.; Alivisatos, A. P. Reaction Chemistry and Ligand Exchange at Cadmium−Selenide Nanocrystal Surfaces. *J. Am. Chem. Soc.* **2008**, *130*, 12279−12281.

(77) Anderson, N. C.; Hendricks, M. P.; Choi, J. J.; Owen, J. S. Ligand Exchange and the Stoichiometry of Metal Chalcogenide Nanocrystals: Spectroscopic Observation of Facile Metal-Carboxylate Displacement and Binding. *J. Am. Chem. Soc.* **2013**, *135*, 18536−18548.

(78) De Roo, J.; De Keukeleere, K.; Hens, Z.; Van Driessche, I. From Ligands to Binding Motifs and beyond; the Enhanced Versatility of Nanocrystal Surfaces. *Dalton Trans.* **2016**, *45*, 13277−13283.

(79) Knauf, R. R.; Lennox, J. C.; Dempsey, J. L. Quantifying Ligand Exchange Reactions at CdSe Nanocrystal Surfaces. *Chem. Mater.* **2016**, *28*, 4762−4770.

(80) Naiini, A. A.; Young, V.; Verkade, J. G. New Complexes of Triethanolamine (TEA): Novel Structural Features of $[Y(TEA)_2](ClO_4)_3{\cdot}3C_5H_5N$ and $[Cd(TEA)_2](NO_3)_2$. *Polyhedron* **1995**, *14*, 393−400.

(81) Hartley, C. L.; Kessler, M. L.; Dempsey, J. L. Molecular-Level Insight into Semiconductor Nanocrystal Surfaces. *J. Am. Chem. Soc.* **2021**, *143*, 1251−1266.

(82) Hartley, C. L.; Dempsey, J. L. Electron-Promoted X-Type Ligand Displacement at CdSe Quantum Dot Surfaces. *Nano Lett* **2019**, *19*, 1151−1157.

(83) Fritzinger, B.; Moreels, I.; Lommens, P.; Koole, R.; Hens, Z.; Martins, J. C. In Situ Observation of Rapid Ligand Exchange in Colloidal Nanocrystal Suspensions Using Transfer NOE Nuclear Magnetic Resonance Spectroscopy. *J. Am. Chem. Soc.* **2009**, *131*, 3024−3032.

(84) Das, A.; Han, Z.; Haghighi, M. G.; Eisenberg, R. Photogeneration of Hydrogen from Water Using CdSe Nanocrystals Demonstrating the Importance of Surface Exchange. *Proc. Natl. Acad. Sci. U. S. A.* **2013**, *110*, 16716.

Recommended by ACS

Nickel-Catalyzed Electroreductive Coupling of Alkylpyridinium Salts and Aryl Halides

Jiantao Fu, Dipannita Kalyani, *et al.*

JUNE 28, 2023
ACS CATALYSIS

READ

Visible Light-Mediated Quantum Dot Photocatalysis Enables Olefination Reactions at Room Temperature

Indra Narayan Chakraborty, Pramod P. Pillai, *et al.*

MAY 16, 2023
ACS CATALYSIS

READ

Photoredox Cleavage of a C_{sp3}–C_{sp3} Bond in Aromatic Hydrocarbons

Ke Liao, Yong Huang, *et al.*

MAY 22, 2023
JOURNAL OF THE AMERICAN CHEMICAL SOCIETY

READ

Deep Electroreductive Chemistry: Harnessing Carbon- and Silicon-Based Reactive Intermediates in Organic Synthesis

Wen Zhang, Song Lin, *et al.*

MAY 31, 2023
ACS CATALYSIS

READ

Get More Suggestions >

https://doi.org/10.1021/acscatal.3c01984
ACS Catal. 2023, 13, 9018−9024